Terahertz Topological Valley Photonic Crystals with Polymer-Filled Bearded Interface for Robust Waveguiding in 6G Applications

Dibaskar Biswas
Department of Electronics and Electrical Engineering
Indian Institute of Technology Guwahati
Guwahati, Assam, India
dibaskar.biswas@iitg.ac.in

Tushar Shah
Department of Electronics and Electrical Engineering
Indian Institute of Technology Guwahati
Guwahati, Assam, India
tushar.shah@iitg.ac.in

Sourodipto Das
Department of Electronics and Electrical Engineering
Indian Institute of Technology Guwahati
Guwahati, Assam, India
d.sourodipto@iitg.ac.in

Amit Baran Dey
Department of Electronics and Electrical Engineering
Indian Institute of Technology Guwahati
Guwahati, Assam, India
deyamit@iitg.ac.in

Ashish Kumar Chowdhary
Department of Electronics and Communication Engineering
Indian Institute of Technology Roorkee
Roorkee, Uttarakhand, India
ashish.chowdhary@ece.iitr.ac.in

Debabrata Sikdar
Department of Electronics and Electrical Engineering
Indian Institute of Technology Guwahati
Guwahati, Assam, India
deb.sikdar@iitg.ac.in

***Abstract*—The discovery of topological insulators caused a significant stir in the scientific community, drawing the attention of numerous researchers from all over the world. The resulting surge of interest progressively spread to the field of photonics, which holds the potential to completely transform the way light is controlled and manipulated. Topological Valley Photonic Crystals (VPCs), offer superior and robust transmission than their equivalent counterparts, owing to the presence of robust topological edge states. In the terahertz frequency range, backscattering disturbances that result in energy losses and signal distortion are present in all traditional photonic crystal-based devices. Here, a terahertz (THz) topological valley photonic waveguide operating within 320–350 GHz is shown, where a polymer-filled bearded interface minimises propagation loss commonly inherent to conventional zig-zag and bearded interfaces. Selective filling of air holes of bearded interface throughout the waveguide path with polyethylene terephthalate (PET) re-positions edge modes away from the bulk bands thereby minimising bulk-edge mode hybridization and improving impedance matching at the coupling interface. This novel approach yields a transmission efficiency of $\sim$ 90%, surpassing the $\sim$ 80% efficiency of previous THz coupling approaches. The proposed design has propagation and bending loss coefficients of 0.2307 dB/cm and 0.0621 dB/bend, respectively. Consequently, these exceptional low-loss characteristics demonstrate the immense potential of polymer-augmented topological waveguides in realizing high-density, robust terahertz integrated circuits for next-generation 6G communication systems**

***Index Terms*—Topological edge states, valley photonic crystals, Berry curvature, Chern number.**

I. Introduction

Topological photonics is an emerging area that has attracted attention because it prevents backscattering, ensuring that light flows efficiently across sharp bends and corners [1], [2]. In topological insulators, one of the most important features was that the edge states are topologically protected and propagate only along the interface of bulk materials, while the bulk itself remains non-conducting [3]. The topological behavior was first demonstrated in electronic systems and was theoretically assumed to be extended to photonic systems since the wave nature of photons in a crystal is fairly similar to that of electrons in solid systems [4], [5]. Extensive studies, including time reversal (TR) symmetry breaking with the help of either magnetic field or artificial gauge potential, demonstrated the emergence of edge states. Further research into this domain threw light on the implementation of the edge states even without the need for external fields. Then these robust topological edge modes were observed in all-dielectric photonic crystals (PC) configured in hexagonal asymmetric lattices [6], [7], [8], [9]. Introducing asymmetry into hexagonal lattice structures resulted in the emergence of edge states, paving the way for intriguing applications in the field of photonic devices [10], [11], [12], [13]. Given the current demand for high-speed data processing in communication systems, the efficient routing of data signals through multiple pathways has become increasingly crucial. The implementation of such paths demands robust, low-loss and high bandwidth wave-guides[12], [14]. Terahertz (1 THz = 10^{12} Hz) frequencies offer a wide spectral bandwidth essential for terabit per second (Tbps) links, driving advances in ultrafast wireless networks such as 6G and beyond. Their short wavelengths enable highly directed communication, compact device components, and precise 3D positioning, supporting the 6G goals of seamless sensing, low latency, and energy efficiency [15], [16]. The requirement of lossless

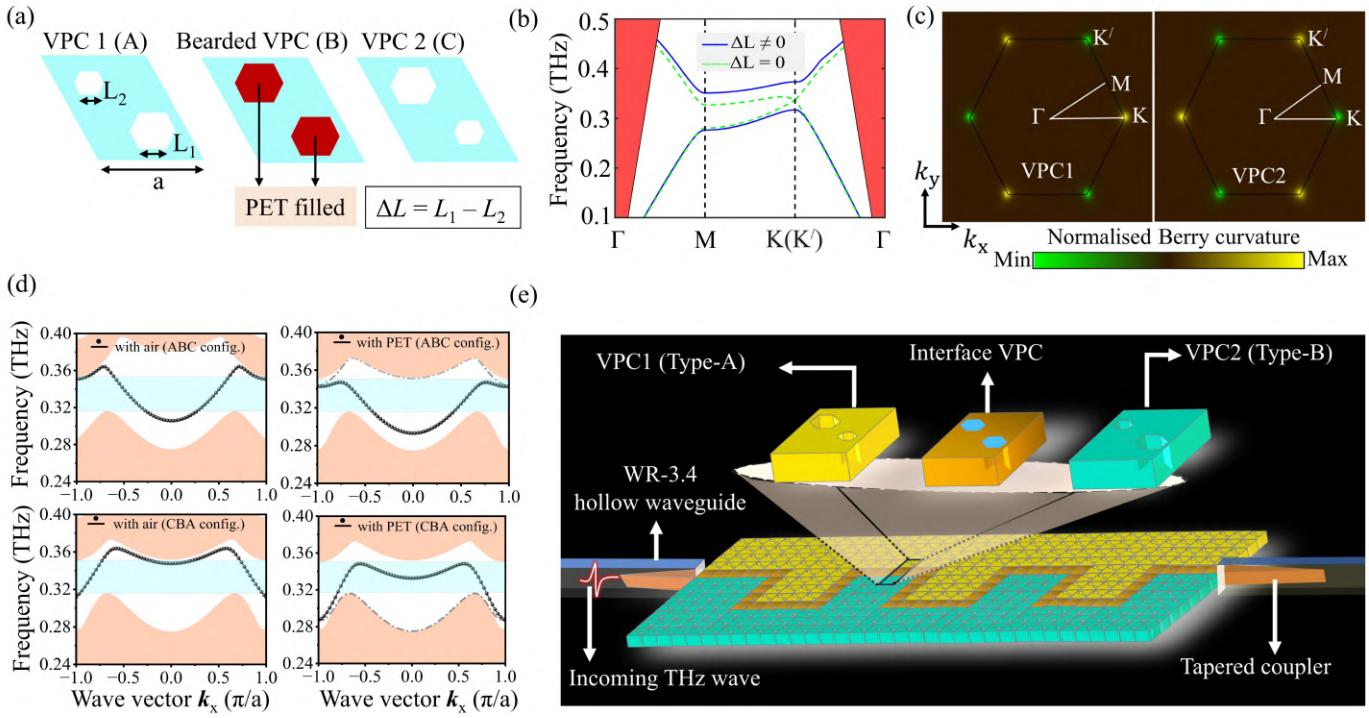

Fig. 1. (a) Schematic representation of the VPC unit cells, the bearded VPC being the interface between VPC1 and VPC2. (b) Photonic band diagram for the VPC unit cell. The green curves correspond to the inversion symmetric unit cell which forms the Dirac cone while the blue curves represent VPC cells with broken inversion symmetry. (c) Berry curvature plot showing the entire Brillouin zone for VPC1 and VPC2 with the topological transitions at the K and $K^{/}$ points. (d) Projected dispersion states with (left) air and (right) PET cladding. The orange and cyan coloured regions represent bulk states and topological bandgap. The dashed line near bulk regions represents the non-topological mode. (e) Schematic representation of the proposed waveguide design. The red path is the PET filled bearded interface which assists the THz transmission coupled through the tapers. Inset of a portion of the waveguide structure showing the placement of VPC1, bearded VPC and VPC2.

waveguides at sharp corners and defects was fulfilled by the topological valley photonic crystals (VPCs). At the boundaries between unit cells of VPCs, topologically protected edge states prevent inter-valley mixing. This development underscores the significant potential of the THz frequency band as a transformative technology for future 6G communications, positioning THz topological valley photonics as a practical approach to maximize its capabilities. VPCs using all-dielectric materials can exhibit a topological phenomenon by breaking the unit cell symmetry. They can also be conveniently fabricated with all-dielectric materials on a chip that is compatible with CMOS technology. In this paper, we propose a high-efficiency, THz topological waveguide design based on a novel polymer filled bearded interface where the conventional transmission ceiling is surpassed. To overcome the propagation losses inherent in conventional air-hole designs, we introduce PET material into the void spaces of the bearded interface. This structural innovation significantly improves signal confinement and transport. Our analysis reveals that the bearded-PET interface achieves a maximum transmission efficiency of 89.94%, compared to the peak efficiencies of 79.6% and 79.25% of bearded filled air and conventional zigzag interfaces, respectively. Quantitative analysis of the proposed VPC waveguide confirms the high transmission efficiency and robustness against sharp corners, yielding a propagation loss of only 0.2307 dB/cm and a bend loss coefficient of 0.0621 dB/bend.

II. Design and Simulation

We employ a high-resistivity silicon slab ($h = 200\,\mu$m) with a rhombic lattice of $a = 242.5\,\mu$m. Inversion symmetry is broken by unequal hexagonal holes ($L_1 = 0.5a$, $L_2 = 0.275a$) placed on either sides of the shorter diagonal of rhombus. The asymmetry parameter $\Delta = L_1 - L_2$ defines two configurations (VPC1 ($\Delta > 0$) and VPC2 ($\Delta < 0$)), which bounds a inversion symmetric bearded interface ($\Delta = 0$) (see Fig. 1(a)). Symmetry breaking lifts the K-point degeneracy at 310 GHz, opening a bandgap from 320 to 350 GHz (Fig. 1(b)). This topological phase transition is characterized by the accumulation of the geometric (Berry) phase [17]. Numerical computation of the Berry curvature confirms non-zero values at the high-symmetry points across the Brillouin zone (Fig. 1(c)), validating topological nature of the proposed unit cell. The PET-filled, bearded holes provide a controlled form of *dielectric loading* for the topological interface, raising the local effective permittivity and thus modifying the modal effective index encountered by the valley-dependent edge modes. In honeycomb photonic crystals, the bands near the Brillouin-zone edge points K and K' (corresponding to $k_x = \pm 2\pi/3a$ in the projected dispersion plot of Fig. 1(d)) can be rigorously explained by a valley-Dirac Hamiltonian, where the introduction of a symmetry-breaking *mass term* opens a gap and

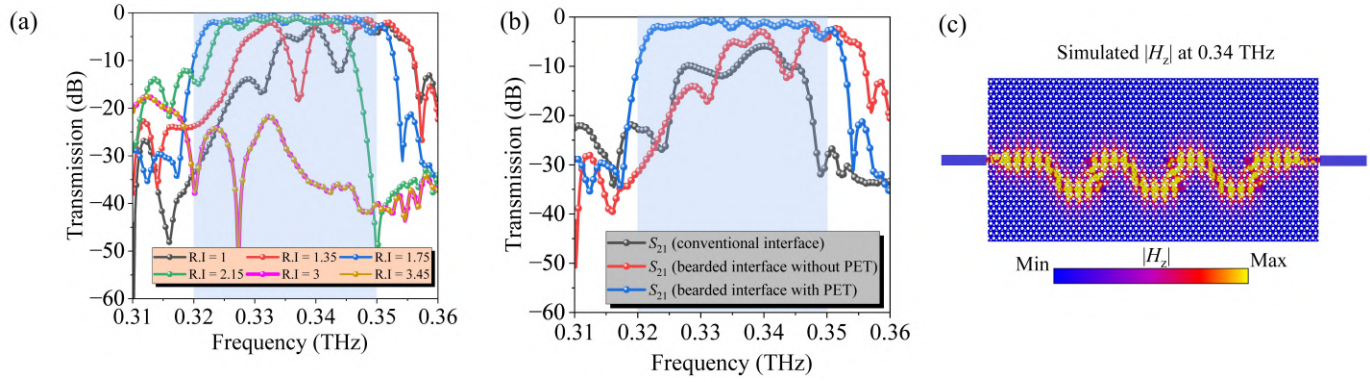

Fig. 2. (a) Parametric analysis showing the transmission spectra for different values of refractive indices of the filled material within bearded voids. (b) Comparison of transmission profiles for different interfaces. (c) Simulated z-component of magnetic field profile H_z at 0.34 THz

localizes Berry curvature with opposite sign in the two distinct valleys. A standard form of the Dirac Hamiltonian equation is given by [18]:

$$H_\tau(\mathbf{q}) = v_D\,(\tau q_x \sigma_x + q_y \sigma_y) + m\,\sigma_z, \tag{1}$$

Here, $\tau = \pm 1$ denotes the K/K' valleys (located at $k_x = \pm 2\pi/3a$), $\mathbf{q}$ represents momentum measured relative to the valley center, and m is the Dirac mass that generates the valley gap and determines the valley-dependent Berry phase. In the air-clad configuration, the edge mode located near K/K' sits closer to the projected bulk bands, which facilitates bulk–edge mixing. PET inclusion imposes a dielectric loading on the bearded holes, effectively renormalizing the local valley-Dirac parameters and shifting the edge dispersion further into the bandgap at K/K'. This suppresses radiation leakage while maintaining valley-Hall-guided transport.The proposed topological waveguide configuration (Fig. 1(e)), enables highly efficient coupling of THz modes across the bearded interface.

III. Results and Discussion

Within the 320–350 GHz band, introducing PET ($n_{\mathrm{PET}} \approx 1.75$) into the bearded-interface voids lowers the local refractive index contrast as calculated from the Fresnel reflection [19] ,

$$R = \left(\frac{n_1 - n_2}{n_1 + n_2}\right)^2. \tag{2}$$

The reflection coefficient R at the PET filled bearded interface reduces to $\approx 7.4\%$, which yields a transmission of $T \approx 1 - R \approx 92.6\%$ (assuming negligible absorption). Compared to a conventional zig-zag interface (for which $R \approx 0.30$ and $T \approx 70\%$), PET inclusion provides an absolute transmission enhancement of $\approx 22.6\%$. Furthermore, the selection of PET is not incidental: an extensive parametric exploration of the refractive index of the void-filling material ($n = 1$ to 3.45) demonstrated maximum transmission enhancement (see fig. 2(a)) at the value of $n \approx 1.75$. Consequently, PET emerges as the most suitable impedance-matching filler for the bearded interface. Figure 2(b) compares transmission for multiple interface configurations, showing superior performance for the proposed interface. The field profile is shown in fig. 2(c).

PET can be integrated after the silicon chip is fabricated, avoiding any CMOS foundry contamination concerns. This hybrid approach is a forward-looking methodology with strong precedent, as demonstrated by the successful integration of other functional materials like thin-film lithium niobate and various polymers with silicon platforms [19], [20], [21], [22],

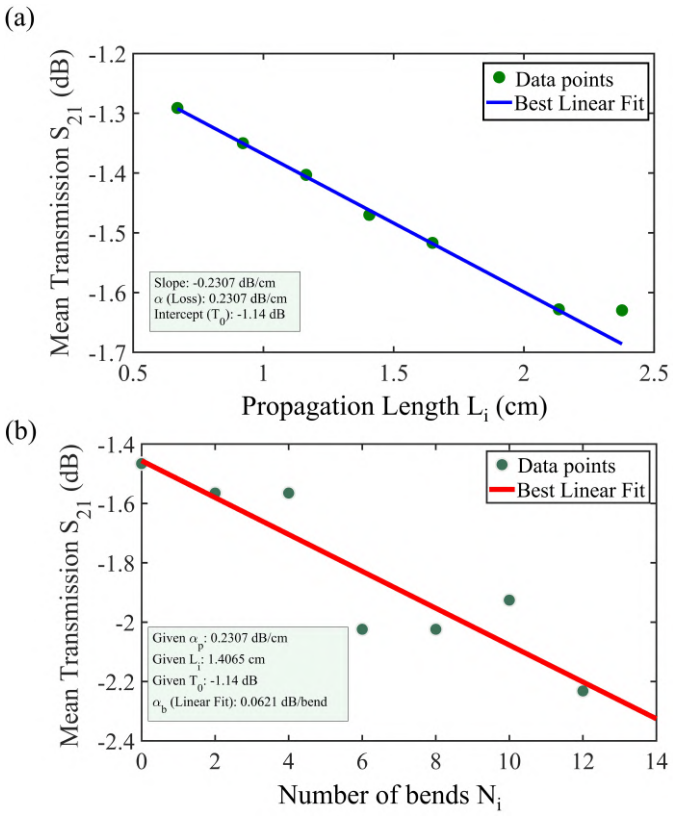

Fig. 3. Transmission as a function of (a) propagation lengths.(b) bending angles at a given device length of $L_i = 1.4065$ cm. The red and blue lines represent the linear fit used for estimating slope and thereby the propagation and bending loss coefficients.

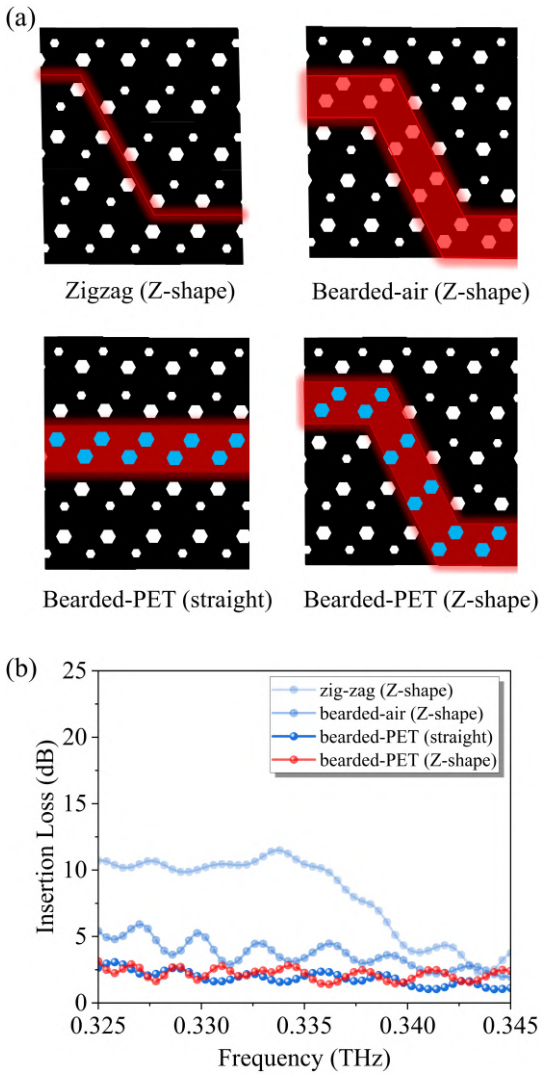

Fig. 4. (a) Schematic representation of different configurations of waveguide interfaces. (b) Insertion Loss as a function of frequency for all the interfaces shown in (a).

[23]. Moreover, in the sub-THz range also, similar polymer integration work has been reported [24]. The physical integration of PET can be achieved via established post-processing techniques like inkjet printing [25].

To quantify the performance of the proposed VPC architecture, the propagation and bending loss characteristics have been evaluated. The total transmission loss (T, in dB) for a waveguide with a specific transmission distance (L_i) and a number of sharp turning bends (N_i) can be generally expressed as:[26]

$$T = T_0 - \alpha_p L_i - \alpha_b N_i \tag{3}$$

where T_0 represents the fixed transmission loss arising from the input/output coupling efficiency, α_p and α_b represents the propagation loss and bending loss coefficients respectively.

We consider the propagation loss first, where the transmission distance (L_i) of a straight topological waveguide configuration is varied, keeping the number of bends as zero

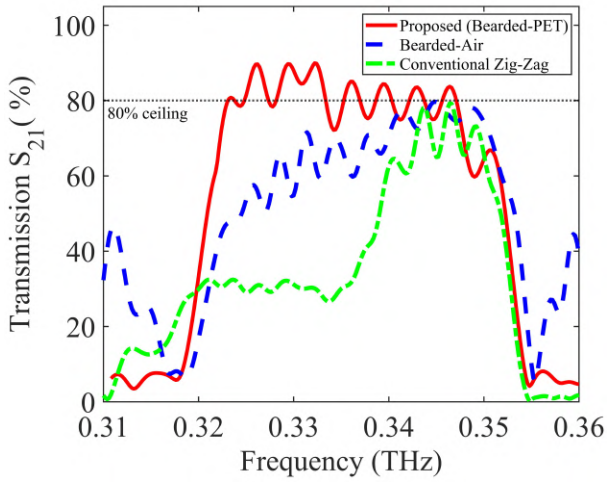

Fig. 5. Comparison of transmission efficieny for different interface configurations.

($N = 0$). Under these conditions, the transmission equation is given by:[26]

$$T_i = T_0 - \alpha_p L_i \tag{4}$$

In fig. 3(a), the mean transmission (S_{21}) is calculated over the operating bandwidth and is plotted as a function of the propagation length L_i. Applying a linear fit algorithm to the measured data points, a steady reduction in total transmission is observed as the distance increases. The slope of this linearly fitted curve provides a direct estimation of the propagation loss. From the fitted curve, the propagation loss coefficient is calculated to be $\alpha_p = 0.2307$ dB/cm, the y-intercept indicating a fixed coupling loss of $T_0 = -1.14$ dB. To calculate the coefficient of bending loss, the transmission response is evaluated by varying the number of bends (N_i) from 0 to 14, at a fixed propagation length of $L_i = 1.4065$ cm. The governing equation for this scenario is given by: [26]

$$T = T_0 - \alpha_p L_i - \alpha_b N_i \tag{5}$$

As depicted in fig. 3(b), using the parameters extracted previously for T_0 and α_p, the mean transmission is plotted against the number of bends N_i. The linearly fitted curve of these measured data points yields a remarkably low bending loss coefficient of $\alpha_b = 0.0621$ dB/bend. These results validate that the proposed topological design is highly efficient and maintains robust transmission stability even when propagating through multiple sharp corners.

To further evaluate the broadband performance of the proposed VPC waveguide and its practical feasibility, we investigate the spectral dependence of the insertion loss. In fig. 4, the insertion loss as a function of frequency is presented in terms of the magnitude of the S_{21} transmission coefficient. The average insertion loss over 320–350 GHz is found to be about 1.59 dB (Straight bearded-PET) and 1.97 dB (Z-shaped bearded-PET). The large portion of this loss is due to the coupling loss that occurs at each of the input and output interfaces of the device. Additionally, the lack of significant transmission

minima or resonant fluctuation in the transmission level within this frequency window provides additional evidence of the robust back-scattering immunity of the topologically protected edge states. Therefore, the small and uniform insertion loss over a wide frequency range indicates the applicability of the proposed VPC platform for high efficiency integrated photonic applications. In fig. 5, the three different waveguiding interface configurations are taken into consideration. The transmission data (S_{21}) were exported from CST Microwave Studio® in linear form and then post processed in MATLAB. Previous THz interconnects commonly exhibit broadband efficiencies of $\sim 80\%$ [27]. In contrast, our first simulation based demonstration of hybrid semiconductor–polymer integration surpasses the $\sim 80\%$ level. The peak transmission noted was 89.994 at 332.20 GHz and an average transmission of 81.8 over the operating bandwidth.

IV. Conclusion

In summary, a THz topological waveguide is presented in which PET-filled bearded holes improve impedance matching at the coupling interface and induce a red-shift to the edge state frequencies at the K/K' points ($k_x = \pm 2\pi/3a$). The potential benefit of this novel semiconductor-polymer hybrid approach has been thoroughly discussed by a set of rigorous simulations —a propagation loss of 0.2307 dB/cm, bending loss of only 0.0621 dB/bend, and a peak transmission of $\sim 90\%$ was achieved compared to the conventional $\sim 80\%$ ceiling level. The proposed topologically protected waveguiding scheme, employing a novel hybrid semiconductor–polymer platform, shows strong promise for active components in future 6G technologies.

Acknowledgment

This work was supported by the Prime Minister's Research Fellowship (PMRF, MoE, Government of India) and the TTDF/6G/328 Project Grant (DoT, Government of India).

References

[1] S. Raghu and F. D. M. Haldane, "Analogs of quantum-hall-effect edge states in photonic crystals," *Phys. Rev. A*, vol. 78, p. 033834, Sep 2008.

[2] K. v. Klitzing, G. Dorda, and M. Pepper, "New method for high-accuracy determination of the fine-structure constant based on quantized hall resistance," *Phys. Rev. Lett.*, vol. 45, pp. 494–497, Aug 1980.

[3] F. D. M. Haldane and S. Raghu, "Possible realization of directional optical waveguides in photonic crystals with broken time-reversal symmetry," *Phys. Rev. Lett.*, vol. 100, p. 013904, Jan 2008.

[4] M. Z. Hasan and C. L. Kane, "Colloquium: Topological insulators," *Rev. Mod. Phys.*, vol. 82, pp. 3045–3067, Nov 2010.

[5] A. B. Khanikaev and G. Shvets, "Two-dimensional topological photonics," *Nature photonics*, vol. 11, no. 12, pp. 763–773, 2017.

[6] X. Xu, X. Li, J. Yang, Y. Zhao, H. Liu, D. Yan, J. Liu, and W. Zhou, "Polymer valley photonic crystals with honeycomb structures for terahertz waveguides," *Optics Communications*, vol. 538, p. 129446, 2023.

[7] A. Shi, B. Yan, R. Ge, J. Xie, Y. Peng, H. Li, W. E. I. Sha, and J. Liu, "Coupled cavity-waveguide based on topological corner state and edge state," *Opt. Lett.*, vol. 46, no. 5, pp. 1089–1092, Mar 2021.

[8] Y. Shen, J. Ji, H.-C. Li, L. Zhang, X. Yu, S.-B. Yan, M. Rasmussen, Q. Shen, D. Madhi, B.-B. Zhou, P. U. Jepsen, and X.-H. Deng, "Realization of photonic topological insulators at terahertz frequencies characterized by time-domain spectroscopy," *Phys. Rev. Appl.*, vol. 18, p. 064025, Dec 2022.

[9] J. Chen, W. Liang, and Z.-Y. Li, "Switchable slow light rainbow trapping and releasing in strongly coupling topological photonic systems," *Photon. Res.*, vol. 7, no. 9, pp. 1075–1080, Sep 2019.

[10] J. Webber, Y. Yamagami, G. Ducournau, P. Szriftgiser, K. Iyoda, M. Fujita, T. Nagatsuma, and R. Singh, "Terahertz band communications with topological valley photonic crystal waveguide," *Journal of Lightwave Technology*, vol. 39, no. 24, pp. 7609–7620, Dec 2021.

[11] X.-T. He, E.-T. Liang, J.-J. Yuan, H.-Y. Qiu, X.-D. Chen, F.-L. Zhao, and J.-W. Dong, "A silicon-on-insulator slab for topological valley transport," *Nature communications*, vol. 10, no. 1, p. 872, 2019.

[12] Y. Yang, Y. Yamagami, X. Yu, P. Pitchappa, J. Webber, B. Zhang, M. Fujita, T. Nagatsuma, and R. Singh, "Terahertz topological photonics for on-chip communication," *Nature Photonics*, vol. 14, no. 7, pp. 446–451, 2020.

[13] D. Biswas, S. Das, and D. Sikdar, "Actively tunable wideband terahertz topological power splitter with customizable splitting ratio," *Journal of Physics D: Applied Physics*, vol. 59, no. 8, p. 085107, 2026.

[14] R. Kumar, R. K. M., S. Pandey, S. K. Srivastava, and G. Kumar, "Terahertz tunable band-stop filter using topological valley photonic crystals," *Appl. Opt.*, vol. 63, no. 1, pp. 104–111, Jan 2024.

[15] S. Vincent and A. Kumar Chowdhary, "Design of tunable metasurfaces for ultra-broadband absorption in terahertz imaging applications," *Journal of Physics D: Applied Physics*, vol. 58, no. 33, p. 335101, 2025.

[16] A. Kumari, S. Vincent, and A. K. Chowdhary, "Ultra-sensitive wide-angle and polarization-independent terahertz metamaterial absorbers for early detection of basal cell carcinoma," *Physica Scripta*, vol. 100, no. 10, p. 105536, 2025.

[17] D. Bisharat, R. Davis, Y. Zhou, P. Bandaru, and D. Sievenpiper, "Photonic topological insulators: A beginner's introduction [electromagnetic perspectives]," *IEEE Antennas and Propagation Magazine*, vol. 63, no. 3, pp. 112–124, June 2021.

[18] T. Ozawa, H. M. Price, A. Amo, N. Goldman, M. Hafezi, L. Lu, M. C. Rechtsman, D. Schuster, J. Simon, O. Zilberberg *et al.*, "Topological photonics," *Reviews of Modern Physics*, vol. 91, no. 1, p. 015006, 2019.

[19] M. He, M. Xu, Y. Ren, J. Jian, Z. Ruan, Y. Xu, S. Gao, S. Sun, X. Wen, L. Zhou *et al.*, "High-performance hybrid silicon and lithium niobate mach–zehnder modulators for 100 gbit s- 1 and beyond," *Nature photonics*, vol. 13, no. 5, pp. 359–364, 2019.

[20] I. Taghavi, M. Moridsadat, A. Tofini, S. Raza, N. A. Jaeger, L. Chrostowski, B. J. Shastri, and S. Shekhar, "Polymer modulators in silicon photonics: review and projections," *Nanophotonics*, vol. 11, no. 17, pp. 3855–3871, 2022.

[21] Z. Gao, Y. Du, Q. Zhang, Y. Qin, J. Fang, and Y. Yi, "Silica–polymer heterogeneous hybrid integrated mach–zehnder interferometer optical waveguide temperature sensor," *Polymers*, vol. 16, no. 16, p. 2297, 2024.

[22] S. Shekhar, W. Bogaerts, L. Chrostowski, J. E. Bowers, M. Hochberg, R. Soref, and B. J. Shastri, "Roadmapping the next generation of silicon photonics," *Nature Communications*, vol. 15, no. 1, p. 751, 2024.

[23] C. Koos, J. Leuthold, W. Freude, M. Kohl, L. Dalton, W. Bogaerts, A. L. Giesecke, M. Lauermann, A. Melikyan, S. Koeber *et al.*, "Silicon-organic hybrid (soh) and plasmonic-organic hybrid (poh) integration," *Journal of Lightwave Technology*, vol. 34, no. 2, pp. 256–268, 2015.

[24] M. Burla, C. Hoessbacher, W. Heni, C. Haffner, Y. Fedoryshyn, D. Werner, T. Watanabe, H. Massler, D. L. Elder, L. R. Dalton *et al.*, "500 ghz plasmonic mach-zehnder modulator enabling sub-thz microwave photonics," *Apl Photonics*, vol. 4, no. 5, 2019.

[25] K. Yan, J. Li, L. Pan, and Y. Shi, "Inkjet printing for flexible and wearable electronics," *Apl Materials*, vol. 8, no. 12, 2020.

[26] G. Jena, N. Chourasis, R. K. Singh, R. K. Varshney, and D. Roy Chowdhury, "Valley assisted and topologically protected dispersion-less beam splitter in microwave photonic crystal," *Journal of Physics D: Applied Physics*, vol. 59, no. 2, p. 025101, 2026.

[27] B. Shi, Q. Jia, X. Li, Y. Zhang, H. Li, Y. Gao, W. Gao, X. Li, D. Tang, T. Zhu *et al.*, "Efficient coupling of topological photonic crystal waveguides based on transverse spin matching mechanism," *Nature Communications*, vol. 16, no. 1, p. 4645, 2025.